

Constraining new physics scenarios in neutrino oscillations from Daya Bay data

I. Girardi¹ and D. Meloni²

¹SISSA/INFN, Via Bonomea 265, I-34136 Trieste, Italy

²Dipartimento di Matematica e Fisica, Università di Roma Tre, Via della Vasca Navale 84, I-00146 Rome

(Dated: June 17, 2021)

We perform for the first time a detailed fit to the $\bar{\nu}_e \rightarrow \bar{\nu}_e$ disappearance data of the Daya Bay experiment to constrain the parameter space of models where sterile neutrinos can propagate in a large compactified extra dimension (LED) and models where non-standard interactions affect the neutrino production and detection (NSI). We find that the compactification radius R in LED scenarios can be constrained at the level of $0.57 \mu m$ for normal ordering and of $0.19 \mu m$ for inverted ordering, at 2σ confidence level. For the NSI model, reactor data put a strong upper bound on the parameter ε_{ee} at the level of $\sim 10^{-3}$, whereas the main effect of $\varepsilon_{e\mu}$ and $\varepsilon_{e\tau}$ is a worsening of the determination of θ_{13} .

PACS numbers: 14.60.Pq, 14.60.St, 14.80.Rt

Keywords: non-standard neutrino oscillation, neutrino mixing

After the recent measure of the reactor angle by T2K [1], Daya Bay [2] and Reno [3] experiments, the standard picture of neutrino oscillation seems now to be very well established, with only few items to be clarified, namely the presence of CP violation in the PMNS mixing matrix and the ordering of the mass eigenvalues. Beyond this standard picture, the possibility that new physics can affect neutrino oscillation is not excluded and, although expected to be small, deserve a closer look. A popular interesting model of new physics in neutrino oscillations is the one where sterile neutrinos can propagate, as well as gravity, in large δ compactified extra dimensions (LED) [4] whereas the Standard Model (SM) left-handed neutrinos are confined to a four-dimensional spacetime brane [5–7]. Experiments based on the torsion pendulum instrument set an upper limit on the largest compactification radius $R < 37 \mu m$ for $\delta = 2$ at 95% CL [8]. Much stronger bounds can be set by astrophysics [9] but they are not completely model independent, so an analysis of the constraints coming from neutrino oscillation data still deserves a lot of attention. Since scenarios with only one extra dimensions have been already ruled-out [8], we assume to work with an effective 5-dimensional theory in which only the radius R of the largest new dimension is the relevant parameter for neutrino oscillation. Under these assumptions, the transition amplitude $\bar{\nu}_e \rightarrow \bar{\nu}_e$ in vacuum is given by [7]:

$$A_{ee}(L) = \sum_{i=1}^3 \sum_{n=0}^{\infty} U^{ei} U^{*ei} [U_i^{0n}]^2 \exp \left(i \frac{\lambda_i^{(n)2} L}{2E_\nu R^2} \right), \quad (1)$$

where U^{ei} is the first row of the U_{PMNS} matrix, $\lambda_i^{(n)}$ are the eigenvalues of the neutrino mass ma-

trix given by $\lambda_i^{(n)} \simeq \xi_i/\sqrt{2}$ for $n = 0$ and $\lambda_i \simeq n + \xi_i^2/(2n)$ for $n \geq 1$, with $\xi_i \equiv \sqrt{2}m_i R$ (m_i = absolute neutrino masses) and U_i^{0n} are the elements of the matrix describing the transition between the zero mode and the n -th Kaluza-Klein states [7], $(U_i^{0n})^2 \simeq \xi_i^2/n^2$. For the normal ordering (NO) we assume $m_3 > m_2 > m_1 = m_0$, whereas for the inverted ordering (IO) $m_2 > m_1 > m_3 = m_0$. We note that the effect of LED is significant more pronounced in IO than NO because the latter amplitude $A_{ee}^{NO}(L) \sim \xi_1^2 U_{e1}^2 + \xi_2^2 U_{e2}^2 + \xi_3^2 U_{e3}^2$ is dominated by $\xi_3^2 \sin^2 \theta_{13}$, then suppressed by θ_{13} , whereas in the IO $A_{ee}^{IO}(L) \sim \xi_1^2 U_{e1}^2 + \xi_2^2 U_{e2}^2$ and does not suffer of such a suppression. We then expect the IO scenario to give better constraints on R and m_0 than the NO case.

Another interesting model of physics beyond the standard three neutrino oscillation is the one called non-standard neutrino interactions (NSI) [10], in which new physics effects can appear at low energy in terms of unknown couplings $\varepsilon_{\alpha\beta}$, generated after integrating out new degrees of freedom, with very large mass scales. In reactor experiments, the new couplings can affect neutrino production ("s") and detection ("d") [11], so the neutrino states are a superposition of pure orthonormal flavor eigenstates [12, 13] according to: $|\nu_e^s\rangle = [(1 + \varepsilon^s)|\nu\rangle]_e$ and $\langle\nu_e^d| = [\langle\nu|(1 + \varepsilon^d)]_e$, with ε^s and ε^d generic non-unitary transformations. Since the parameters $\varepsilon_{e\alpha}^s$ and $\varepsilon_{e\alpha}^d$ receive contributions from the same higher dimensional operators [14], one can constrain them by the relation $\varepsilon_{e\alpha}^s = \varepsilon_{e\alpha}^{d*} \equiv \varepsilon_{e\alpha} e^{i\phi_{e\alpha}}$, being $\varepsilon_{e\alpha}$ the modulus and $\phi_{e\alpha}$ the argument of $\varepsilon_{e\alpha}^s$. The oscillation probability $P_{ee} \equiv P(\bar{\nu}_e \rightarrow \bar{\nu}_e)$ up

to $O(\varepsilon)$ can be obtained by squaring the amplitude $\langle \nu_e^d | e^{-iHL} | \nu_e^s \rangle$:

$$P_{ee} = 1 - \sin^2 2\theta_{13} \sin^2 \Delta + 4\varepsilon_{ee} \cos \phi_{ee} \quad (2) \\ - 4\varepsilon_{e\mu} \sin 2\theta_{13} \sin \theta_{23} \cos 2\theta_{13} \cos(\delta - \phi_{e\mu}) \sin^2 \Delta \\ - 4\varepsilon_{e\tau} \sin 2\theta_{13} \cos \theta_{23} \cos 2\theta_{13} \cos(\delta - \phi_{e\tau}) \sin^2 \Delta,$$

where $\Delta \equiv \left[\frac{\Delta m_{31}^2 L}{4E_\nu} \right]$, with L being the source-to-detector distance, E_ν the neutrino energy and $\Delta m_{31}^2 = m_3^2 - m_1^2$. In the first line of Eq. (2) we can recognize the "zero-distance" term driven by ε_{ee} , which gives a non vanishing contribution even in the limit of very small L/E_ν . In addition, $\varepsilon_{e\mu}$ and $\varepsilon_{e\tau}$ appear with only slightly different coefficients. However, contrary to what happens for ε_{ee} , $\varepsilon_{e\mu, \tau}$ exhibit a strong correlation with the reactor angle which, on the one hand, does not allow to set any stringent bound on them and, on the other hand, can worsen the extraction of θ_{13} and Δm_{31}^2 from the data [15, 16]. A model-independent analysis [17] has shown that all bounds on production and detection NSI's are at the level of 10^{-2} : $\varepsilon_{ee} < 0.041$, $\varepsilon_{e\mu} < 0.025$ and $\varepsilon_{e\tau} < 0.041$, whereas for the CP violating phases no constraints are known.

In this paper we make use of the recent $\bar{\nu}_e \rightarrow \bar{\nu}_e$ disappearance data of the Daya Bay experiment to constrain the parameter space of NSI and LED scenarios. Our main results are that neutrino oscillation data can provide strong upper bounds on ε_{ee} at the level of $\mathcal{O}(10^{-3})$, whereas for R the exclusion limits are between 1 and 2 order of magnitudes below the limits quoted in [8].

The Daya Bay experimental setup we take into account [2] consists of six antineutrino detectors (ADs) and six reactors, D1, D2, L1, L2, L3, L4. The antineutrino spectra emitted by the nuclear reactors have been recently estimated in [18, 19]. For each AD's, the flux of arriving $\bar{\nu}_e$ has contributions from the isotopes ^{235}U , ^{239}Pu , ^{238}U , and ^{241}Pu , with weights reported in [20]; for a given isotope, we adopt the convenient parametrization of [18]. For our analysis we used the data set accumulated during 217 days reported in [21], where the detected antineutrino candidates are collected in the far hall, EH3, and in the near halls EH1, EH2. A bin-to-bin normalization has been fixed in order to reproduce the unoscillated rates. The antineutrino energy $E_{\bar{\nu}_e}$ is reconstructed by the prompt energy deposited by the positron E_{prompt} using the approximated relation [2]: $E_{\bar{\nu}_e} \simeq E_{\text{prompt}} + 0.8 \text{ MeV}$. The energy resolution function is a Gaussian function with $\sigma(E)[\text{MeV}] = 0.08\sqrt{E_\nu/\text{MeV}} - 0.8$. The antineutrino cross section for the inverse beta decay (IBD) process has been taken from [22]. In order

to perform a proper statistical treatment of correlations and degeneracy, we used a modified version of the GLoBES software [23] and construct an adequate definition of the χ^2 function [2]:

$$\chi^2(\theta, \Delta m^2, \vec{S}, \alpha_r, \varepsilon_d, \eta_d) = \\ \sum_{d=1}^6 \sum_{i=1}^{36} \frac{[M_i^d - T_i^d \cdot (1 + \sum_r \omega_r^d \alpha_r + \varepsilon_d) + \eta_d]^2}{M_i^d + B_i^d} \\ + \sum_r \frac{\alpha_r^2}{\sigma_r^2} + \sum_{d=1}^6 \left[\frac{\varepsilon_d^2}{\sigma_d^2} + \frac{\eta_d^2}{\sigma_{B_d}^2} \right] + \text{Priors}. \quad (3)$$

In the previous formula, \vec{S} is a vector containing the new physics parameters, M_i^d are the measured IBD events of the d-th detector ADs in the i-th bin, B_i^d the corresponding background and $T_i^d = T_i(\theta, \Delta m^2, \vec{S})$ are the theoretical prediction for the rates. The parameter ω_r^d is the fraction of IBD contribution of the r-th reactor to the d-th detector AD, determined by the approximated relation $\omega_r^d \sim L_{rd}^{-2} / (\sum_{r=1}^6 1/L_{rd}^2)$, where L_{rd} is the distance between the d-th detector and the r-th reactor. The parameter σ_d is the uncorrelated detection uncertainty ($\sigma_d = 0.2\%$) and σ_{B_d} is the background uncertainty of the d-th detector obtained using the information given in [21]: $\sigma_{B_1} = \sigma_{B_2} = 8.21$, $\sigma_{B_3} = 5.95$, $\sigma_{B_4} = \sigma_{B_5} = \sigma_{B_6} = 1.15$. Eventually, $\sigma_r = 0.8\%$ is the correlated reactor uncertainties. The corresponding pull parameters are $(\varepsilon_d, \eta_d, \alpha_r)$. The main relevant point in this discussion is which priors must be implemented in the fitting function. Since Daya Bay has measured θ_{13} with very high precision, we cannot use its determination to constraint the reactor angle when fitting the new physics parameters, otherwise we would use the same data twice. Similar considerations can also be done for the atmospheric mass difference, which primarily drives the standard oscillation term in P_{ee} . So, when studying LED in the plane (R, m_0) and NSI in the plane $(\varepsilon_{\alpha\beta}, \phi_{\alpha\beta})$, we adopt the following strategy: we do not impose any constraints of θ_{13} and we set the uncertainty on Δm_{31}^2 at values larger than the current determination: $\Delta m_{31}^2 = (2.35 \pm 10\%) \times 10^{-3} \text{ eV}^2$ (we carefully checked that leaving Δm_{31}^2 completely unconstrained our results do not change). For the atmospheric angle and the solar parameters the situation is a bit different since the standard probability does not depend on them; however, they couple to the new physics parameters, both in LED and NSI scenarios, so we need to impose external constraints, chosen as follows [24]: $\sin^2 \theta_{23} = 0.425 \pm 0.029$ for NO and $\sin^2 \theta_{23} = 0.437 \pm 0.173$ for IO, $\Delta m_{21}^2 = (7.54 \pm 0.26) \times 10^{-5} \text{ eV}^2$ and $\sin^2 \theta_{12} = 0.308 \pm 0.017$. Whenever necessary,

the standard CP violating phase δ will be considered as a free parameter.

The results in the standard $[\sin^2 2\theta_{13}, \Delta m_{31}^2]$ -plane, instead, are obtained marginalizing also over R and m_0 for LED and over ε and ϕ for NSI, in the perturbative regions identified by $\xi_i \equiv \sqrt{2}m_i R < 0.2$ and $\varepsilon < 0.041$, while $\phi \in [0, 2\pi]$.

We first consider the bounds on the size of the large extra dimension R and on the lightest neutrino mass, in the $[R, m_0]$ -plane. Our results are shown in left panel of Fig. 1, where we displayed the 1, 2 and 3 σ CL regions. Both ordering of the neutrino masses, and the related values of the χ_{min}^2/dof , have been considered; solid lines refer to the NO whereas the dashed ones refer to the IO. The horizontal dashed line represents the future upper limit on m_0 from the β -decay experiment KATRIN [25]. Since the standard oscillation physics already gives a good fit to the data, small values of R and m_0 are obviously allowed; the correlation existing among these parameters, however, is quite strong and excludes large values of R and m_0 . In particular, bounds on the compactification radius can be set at the level of some units of $10^{-1} \mu\text{m}$: $R < 0.36$ (0.16) at 1 σ , $R < 0.57$ (0.19) at 2 σ and $R < \text{None}$ (0.23) at 3 σ for NO (IO). The best fit points (a circle for NO and a square for IO in Fig. 1) and the related χ_{min}^2/dof have the following values: $R[\mu\text{m}] = 0.04$ (0.032), $m_0[\text{eV}] = 0.16$ (0.20) with $\chi_{min}^2/\text{dof} = 45/106$ (45/106), where the numbers in parenthesis refer to the IO. However, it is worth to mention that they only have an indicative meaning, since the χ^2 function is almost flat in the allowed regions.

It is an interesting question to check whether the new physics parameters introduce some bias in the simultaneous extraction of θ_{13} and Δm_{31}^2 . In the right panel of Fig. 1 we show the 3 σ CL allowed region in the $[\sin^2(2\theta_{13}), \Delta m_{31}^2]$ -plane for NO (solid line), IO (dotted line), and the standard model (dot-dashed line) results. We can appreciate an increase of the allowed θ_{13} and Δm_{31}^2 3 σ CL regions, at the level of 25% toward smaller reactor angles and 5% to larger masses. In Tab. I we summarise the obtained results, reporting the best fit values and 1 σ errors for $\sin^2 2\theta_{13}$, Δm_{31}^2 and the related value χ_{min}^2/dof for the three scenarios shown in Fig. 1.

The parameter space for the NSI investigation is larger than for LED, consisting of the moduli ε_{ee} , $\varepsilon_{e\mu}$, $\varepsilon_{e\tau}$ and the new CP phases ϕ_{ee} , $\phi_{e\mu}$, $\phi_{e\tau}$. The study of the allowed regions in the $[\varepsilon_{ee}, \phi_{ee}]$ -plane is performed marginalizing over all the parameters, including $\varepsilon_{e\mu}$, $\varepsilon_{e\tau}$ and their phases. The result of

Parameter	SM	LED NO	LED IO
$\sin^2 2\theta_{13}$	$0.085^{+0.015}_{-0.016}$	$0.082^{+0.021}_{-0.022}$	$0.078^{+0.018}_{-0.018}$
$\Delta m_{31}^2/10^{-3} [\text{eV}^2]$	$2.69^{+0.27}_{-0.24}$	$2.69^{+0.30}_{-0.25}$	$2.60^{+0.24}_{-0.20}$
χ_{min}^2/dof	43/106	43/106	42/106

TABLE I: *Best fit points and 1 σ errors for $\sin^2 2\theta_{13}$, Δm_{31}^2 and the value of χ_{min}^2/dof . Results are for the SM, the LED NO and LED IO cases.*

such a procedure is presented in the left panel of Fig. 2, where the 1, 2 and 3 σ CL have been displayed, together with the obtained best fit point (circle). The vertical dashed line is at $\varepsilon_{ee} = 0.041$. The results can be easily explained using the approximate probability in Eq. (2): a maximal sensitivity to ε_{ee} is obtained in correspondence of vanishing CP phase; in addition, the symmetry around $\phi_{ee} \sim \pi$ is a trivial consequence of the $\cos \phi_{ee}$ dependence in P_{ee} . Upper bounds on ε_{ee} can be set of the order $\varepsilon_{ee} \lesssim 3 \cdot 10^{-3}$ for $\phi_{ee} \sim 0, 2\pi$, and $\varepsilon_{ee} \lesssim 5 \cdot 10^{-3}$ for $\phi_{ee} \sim \pi$; in both cases, the Daya Bay data significantly lower the existing upper limit on ε_{ee} . The best fit point is: $\varepsilon_{ee} = 0.001$, $\phi_{ee} = 2.5$, with $\chi_{min}^2/\text{dof} = 45/106$. We have checked that, contrary to what described above, the correlation among θ_{13} and $\varepsilon_{e\mu}$, $\varepsilon_{e\tau}$ does not allow to set any interesting bounds on them.

As for the LED case, we are interested in estimating the determination of the reactor angle θ_{13} and the mass difference Δm_{31}^2 in presence of NSI. Driven by the considerations after Eq. (2), we study two different cases, both illustrated in the right panel of Fig. 2; in the case NSI-I (solid line), we set $\varepsilon_{e\mu} = \varepsilon_{e\tau} = 0$ and marginalize over ε_{ee} and ϕ_{ee} . We see that the effect is a variation in the determination of $\sin^2 2\theta_{13}$ of some $\sim 30\%$, and of the mass difference around $\sim 5\%$.

In the case NSI-II (dotted line), we also leave $\varepsilon_{e\mu}$ and $\varepsilon_{e\tau}$ and the related CP phases as free parameters; the impact on the determination of θ_{13} is really large: beside a drift of the best fit point toward larger values, the allowed 3 σ interval covers a broader 3 σ range, $0.013 \lesssim \sin^2(2\theta_{13}) \lesssim 0.22$ at 3 σ . The obtained best fit points and the 1 σ errors for NSI-I and NSI-II are summarised in Tab. II.

In summary, the most recent data of the Daya Bay experiment [21] allow to set strong upper bounds on the new physics parameters involved in LED and NSI scenarios. For the compactification radius R , the limits at 2 σ are $R < 0.19 \mu\text{m}$ for IO and $R < 0.57 \mu\text{m}$ for NO, much stringent that the current limits from torsion pendulum experiments. For

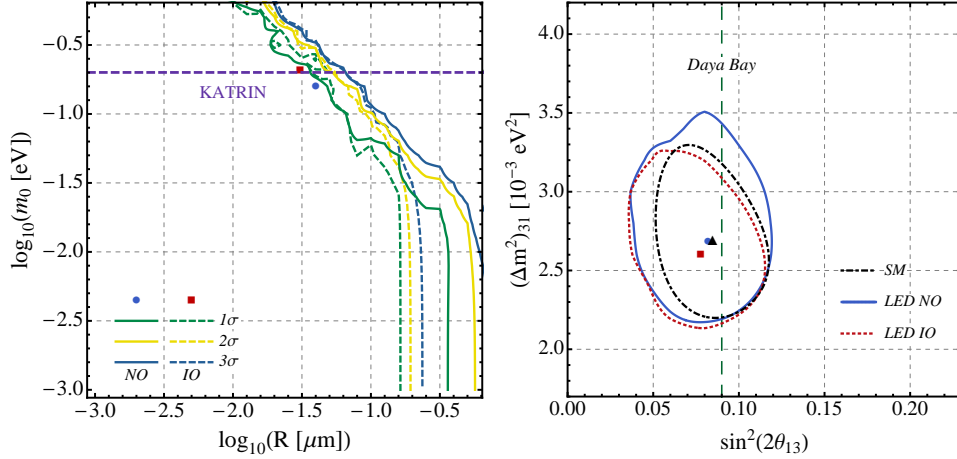


FIG. 1: *Left panel: allowed regions for NO and IO LED model in the $[\log_{10}(R), \log_{10}(m_0)]$ -plane at 1σ , 2σ and 3σ CL. The best fit points for both hierarchies are indicated with a circle (NO) and a square (IO). Right panel: 3σ CL in the $[\sin^2(2\theta_{13}), \Delta m^2_{31}]$ -plane. The best fit points are indicated with a circle (LED NO), a square (LED IO) and a triangle (SM). The dashed vertical line represents the value of the θ_{13} quoted by the Daya Bay collaboration [21].*

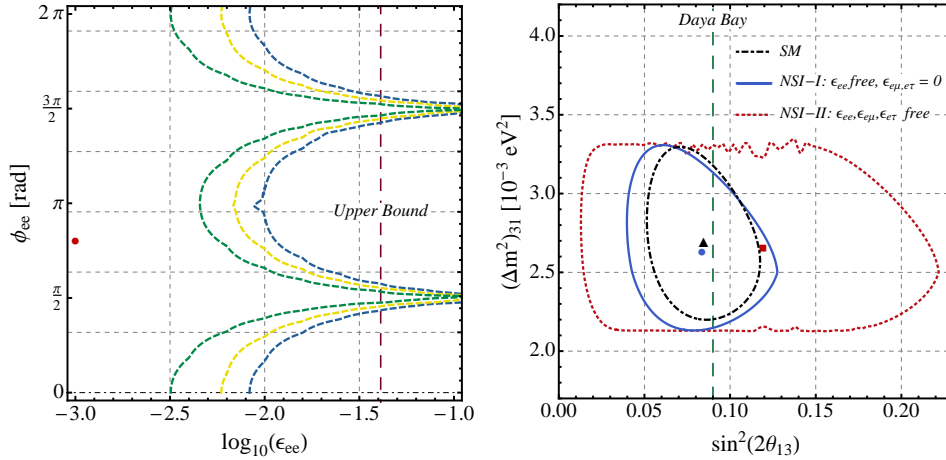


FIG. 2: *Left panel: excluded regions in the $[\epsilon_{ee}, \phi_{ee}]$ -plane at 1 , 2 and 3σ CL. The vertical line corresponds to $\epsilon = 0.041$. Circles are the obtained best fit points. Right Panel: 3σ CL in the $[\sin^2(2\theta_{13}), \Delta m^2_{31}]$ -plane for the SM (dot-dashed), for $\epsilon_{e\mu} = \epsilon_{e\tau} = 0$ (NSI-I solid) and for free parameters (NSI-II dotted). The best fit points are indicated with a circle (NSI-I), a square (NSI-II) and a triangle (SM).*

Parameter	SM	NSI-I	NSI-II
$\sin^2 2\theta_{13}$	$0.085^{+0.015}_{-0.016}$	$0.084^{+0.022}_{-0.021}$	$0.119^{+0.08}_{-0.09}$
$\Delta m^2_{31}/10^{-3} [\text{eV}^2]$	$2.69^{+0.27}_{-0.24}$	$2.62^{+0.30}_{-0.22}$	$2.65^{+0.27}_{-0.25}$
χ^2_{min}/dof	43/106	43/106	43/106

TABLE II: *Best fit points and 1σ errors for $\sin^2 2\theta_{13}$, Δm^2_{31} and the value of χ^2_{min}/dof . Results are for the SM, the NSI-I and NSI-II cases.*

the NSI case, a special role is played by the ϵ_{ee} parameter since it is not correlated to θ_{13} . The experimental data set a strong upper bound of $\mathcal{O}(10^{-3})$

at 3σ . On the other hand, $\epsilon_{e\mu}$ and $\epsilon_{e\tau}$ suffer from a strong correlation to θ_{13} and, therefore, no significant sensitivity has been found. However, they play a major role in the determination of θ_{13} and Δm^2_{31} ; our analysis shows that, even assuming $\epsilon_{ee} = 0$, the allowed regions for θ_{13} are much larger than the SM ones; in addition, the best fit value for θ_{13} is driven to values larger by roughly 40%. On the other hand, the determination of the squared mass difference Δm^2_{31} is less affected by this type of new physics and the fit procedures return values very similar to the SM case.

We acknowledge MIUR (Italy) for financial sup-

port under the program Futuro in Ricerca 2010 (RBFR100360). We are strongly indebted with Patrick Huber and Camillo Mariani for useful discussions on the subtleties of the Daya Bay and Double Chooz experiments and S.T. Petcov for useful suggestions. This work was supported in part by the INFN program on “Astroparticle Physics” and by the European Union FP7-ITN INVISIBLES (Marie Curie Action PITAN-GA-2011-289442-INVISIBLES) (I.G.).

-
- [1] K. Abe et al. (T2K Collaboration), Phys. Rev. Lett. **112**, 061802 (2014).
 - [2] F. P. An et al. (Daya Bay Collaboration), Chin. Phys. C. **37**, 011001 (2013).
 - [3] J. K. An et al. (RENO Collaboration), Phys. Rev. Lett. **108**, 191802 (2012).
 - [4] N. Arkani-Hamed, S. Dimopoulos and G. Dvali, Phys. Lett. B **429**, 263 (1998); I. Antoniadis, N. Arkani-Hamed, S. Dimopoulos and G. Dvali, Phys. Lett. B **436**, 257 (1998); N. Arkani-Hamed, S. Dimopoulos and G. Dvali, Phys. Rev. D **59**, 086004 (1999).
 - [5] R. Barbieri, P. Creminelli and A. Strumia, Nucl. Phys. B **585**, 28 (2000).
 - [6] R. N. Mohapatra, S. Nandi and A. Perez-Lorenzana, Phys. Lett. B **466**, 115 (1999); R. N. Mohapatra and A. Perez-Lorenzana, Nucl. Phys. B **576**, 466 (2000); R. N. Mohapatra and A. Perez-Lorenzana, Nucl. Phys. B **593**, 451 (2001).
 - [7] H. Davoudiasl, P. Langacker and M. Perelstein, Phys. Rev. D **65**, 105015 (2002).
 - [8] J. Beringer et al. (Particle Data Group Collaboration), Phys. Rev. D **86**, 010001 (2012).
 - [9] S. Hannestad and G. G. Raffelt, Phys. Rev. D **67**, 125008 (2003); Erratum-ibid. Phys. Rev. D **69**, 029901 (2004).
 - [10] L. Wolfenstein, Phys. Rev. D **17**, 2369 (1978); M. M. Guzzo, A. Masiero and S. T. Petcov, Phys. Lett. B **260**, 154 (1991).
 - [11] Y. Grossman, Phys. Lett. B **359**, 141 (1995).
 - [12] T. Ohlsson, H. Zhang and S. Zhou, Phys. Lett. B **728**, 148 (2014).
 - [13] D. Meloni, T. Ohlsson, W. Winter and H. Zhang, JHEP **1004**, 041 (2010).
 - [14] J. Kopp, M. Lindner, T. Ota and J. Sato, Phys. Rev. D **77**, 013007 (2008).
 - [15] T. Ohlsson and H. Zhang, Phys. Lett. B **671**, 99 (2009).
 - [16] R. Leitner, M. Malinsky, B. Roskovec and H. Zhang, JHEP **1112**, 001 (2011).
 - [17] C. Biggio, M. Blennow and E. Fernandez-Martinez, JHEP **0908**, 090 (2009).
 - [18] T. A. Mueller et al., Phys. Rev. C **83**, 054615 (2011).
 - [19] P. Huber, Phys. Rev. C **84**, 024617 (2011); Erratum-ibid., Phys. Rev. C **85**, 029901 (2012).
 - [20] S. Jetter, talk given at NuFact13.
 - [21] F. P. An et al. (Daya Bay Collaboration), Phys. Rev. Lett. **112**, 061801 (2014).
 - [22] P. Vogel and J. F. Beacom, Phys. Rev. D **60**, 053003 (1999).
 - [23] P. Huber, J. Kopp, M. Lindner and W. Winter, Comput. Phys. Commun. **167**, 195 (2005); P. Huber, J. Kopp, M. Lindner, M. Rolinec and W. Winter, Comput. Phys. Commun. **177**, 432 (2007).
 - [24] F. Capozzi, G. L. Fogli, E. Lisi, A. Marrone, D. Montanino and A. Palazzo, arXiv:1312.2878.
 - [25] K. Eitel, Nucl. Phys. Proc. Suppl. **143**, 197 (2005).